Hindawi
Science and Technology of Nuclear Installations
Volume 2020, Article ID 4921623, 11 pages
https://doi.org/10.1155/2020/4921623

Research Article

DFT Study of Cs/Sr/Ag Adsorption on Defective Matrix Graphite

Zengtong Jiao,[1] Xiaotong Chen,[1] Chao Fang,[2] Gang Xu,[1] Chi Zhang,[1] Luhao Fan,[1] and Bing Liu[1]

[1]*Institute of Nuclear and New Energy Technology, Tsinghua University, Beijing 100084, China*
[2]*Lab for High Technology, Tsinghua University, Beijing 100084, China*

Correspondence should be addressed to Xiaotong Chen; chenxiaotong@tsinghua.edu.cn and Bing Liu; bingliu@mail.tsinghua.edu.cn

Received 3 December 2019; Revised 24 June 2020; Accepted 1 July 2020; Published 28 August 2020

Academic Editor: Arkady Serikov

Copyright © 2020 Zengtong Jiao et al. This is an open access article distributed under the Creative Commons Attribution License, which permits unrestricted use, distribution, and reproduction in any medium, provided the original work is properly cited.

The geometries, adsorption energies, and electronic structures of Cs, Sr, and Ag atoms on matrix graphite surface with point defects were calculated and analyzed using the density functional theory (DFT) and the Perdew–Burke–Ernzerhof (PBE) formulation of the generalized gradient approximation (GGA). Three different types of point defects, i.e., single vacancy and "bridge" and "spiro" interstitials are considered using approximate van der Waals (vdW) correction methods. The results of adsorption energies show that the metal fission products of Cs, Sr, and Ag are more stable on single vacancy defects than "bridge" or "spiro" interstitial defects. This is further confirmed by the analysis of electronic structures, such as charge density difference (CDD) and density of state (DOS). All these results indicate that dangling bonds play an important role in the adsorption behaviors of metallic fission products on matrix graphite.

1. Introduction

Spherical fuel elements technology of high-temperature gas-cooled reactor (HTGR) effectively enhances the retention capability for fission products and the inherent safety of the reactor especially at high temperature [1, 2]. Tristructural-Isotropic- (TRISO-) [3] coated fuel particles, of which UO_2/UC kernels are coated with carbonaceous buffer layer, inner pyrolytic carbon (IPyC), silicon carbide (SiC), and outer pyrolytic carbon (OPyC) layers, are dispersed in the matrix graphite, as shown in Figure 1. The primary function of these coating layers is to act as diffusion barriers for radioactive fission products to retain fission products within the fuel particles even under accident conditions [4]. However, studies have shown that TRISO-coated fuel particles may be damaged due to pressure shell damage [5], IPyC cracking-induced failures [6], amoeba effect [7], and palladium attack on silicon carbide during the irradiation condition [8]. A substantial amount of key metallic fission products such as Cs, Sr, and Ag may be released from the damaged TRISO-coated fuel particles and adsorbed on the external matrix graphite [9]. In this case, the matrix graphite will become the most important and effective barrier to metallic fission products. Therefore, it is important to understand the adsorption mechanism of fission products on matrix graphite of HTGR spherical fuel element from the atomic scale.

In the past few decades, the adsorption behavior of fission products on carbon materials has been widely studied. Some key parameters of carbon materials, such as atomic structures, sp2-to-sp3 bonding ratio, defect structures, percent of amorphous structures, and porosity, may play a dominant role in fission product sorption [10]. The manufacturing methods, as well as the precursors employed, have an influence on the structure parameters of carbon materials. As a kind of carbon materials, matrix graphite is a mixture of crystalline hexagonal graphite and amorphous carbon originated from phenolic resin binder, which is made from 64 wt% natural flake graphite, 16 wt% electrographite, and 20 wt% phenolic resin binder through specific processing routes [11]. It is inevitable that many defect

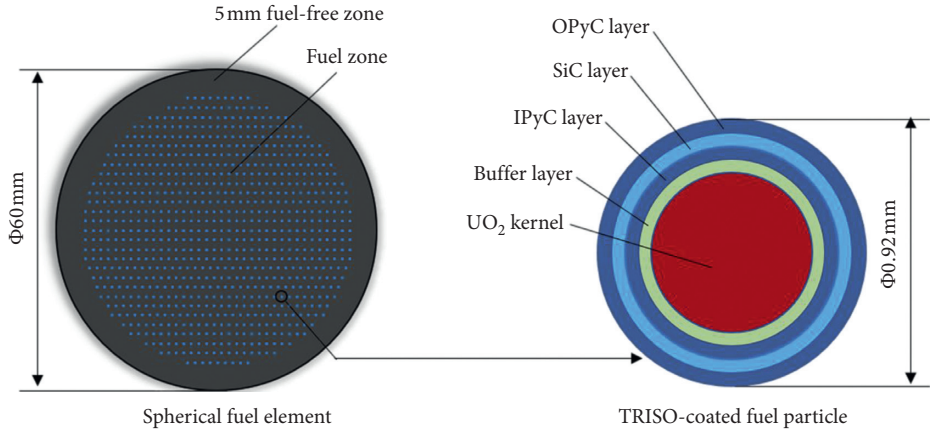

Figure 1: The profiles of spherical fuel element and TRISO-coated fuel particle.

structures will be generated during the preparation and irradiation. The types of defect structures, such as vacancies, interstitials, and Stone–Wales defects, will play a critical role in the adsorption behavior of metallic fission products on matrix graphite [12, 13].

The first-principle calculation based on density functional theory (DFT) provides a method of studying the real adsorption mechanism of three important fission products Cs, Sr, and Ag atoms on the matrix graphite surface with different types of defect structures [14, 15]. Some previous similar work use atoms of fission products [16, 17]. As a simplified model, it is able to obtain the feature of interaction between fission products and graphite and could be used to explain some experimental data [18, 19]. Based on the studies mentioned above, atoms of fission products were used in this study. Londono-Hurtado et al. [20] reported a tendency of graphite with defects and carbons with sp3 bonds to provide much stronger binding energies for Cs and Sr atoms than perfect sp2 graphite using the first-principle calculation. Luo et al. [16] used the DFT method to calculate the adsorption geometry, energy, and electronic structure of four fission products (Cs, Sr, Ag, and I atoms) on the perfect and defective graphite surface with single vacancy. The results show that the graphite surface with single vacancy has stronger adsorption capacity for fission products. Xia et al. [21] further studied the adsorption and diffusion mechanism of metallic fission products (Cs, Sr, and Ag atoms) on the defective graphite surface with double vacancy and Stone–Wales defect by using DFT method. It can be seen from the above that the adsorption behavior of fission products on vacancy defects has been studied, but the interstitial defects have not been fully understood yet. In this work, different kinds of point defects, such as single vacancy and "bridge" and "spiro" interstitials, are examined by the DFT methods accounting for van der Waals (vdW) interactions. Then, we compare the adsorption behavior of fission products (Cs, Sr, and Ag atoms) on the defective graphite surface by analyzing adsorption energies, charge density difference (CDD), and density of state (DOS).

2. Methods and Computational Details

DFT calculations were performed using the Vienna Ab initio Simulation Package (VASP) [22]. The approach implemented in VASP is based on an iterative solution of the Kohn–Sham equation [15] in a plane wave basis set with the projector-augmented wave (PAW) pseudopotentials. Generalized gradient approximation (GGA) in the form of the Perdew–Burke–Ernzerhof (PBE) [23] exchange-correlation (XC) functional was selected in our calculations. Since matrix graphite has a layered, planar structure, the interlayer binding energy calculated by conventional PBE method is too small compared with the available experimental data [24]. However, this problem can be solved if a correction term E_{disp} is added to the conventional Kohn–Sham DFT energy $E_{\text{KS-DFT}}$:

$$E_{\text{DFT-disp}} = E_{\text{KS-DFT}} + E_{\text{disp}}. \quad (1)$$

E_{disp} is calculated by some of the available approximate methods, such as vdW-DF method [25], DFT-D2 method [26], DFT-D3 method [27, 28], Tkatchenko–Scheffler method (TS-SCS) [29], and many-body dispersion energy method (MBD@rsSCS) [30, 31]. Among them, MBD@rsSCS method is the most suitable for graphite systems. In this work, the calculated interlayer binding energy of 49 meV/atom is fairly close to theoretical calculated value of 48 meV/atom [31] and the experimental measured value of 43 ± 5 meV/atom [32]. Without van der Waals correction and using the PW91 exchange-correlation (XC) function as in the previous study [16, 21], the calculated interlayer binding energy is −15 meV, which is much smaller than the experimental and theoretical values.

For the matrix graphite (0001) surface model, we used a 3×3 supercell containing three graphite layers with ABA stacking sequence. The atoms in the lower portion of the supercell is repeated periodically along x- and y-directions, while a 15 Å vacuum space was applied in the top portion of the supercell to exclude interactions between adjacent slabs. For all models considered, the plane-wave cutoff energy was set to 400 eV by [21]. The atomic poisons within the supercell were fully relaxed until the maximal forces were less than 0.02 eV/Å. The self-consistent calculations have been carried

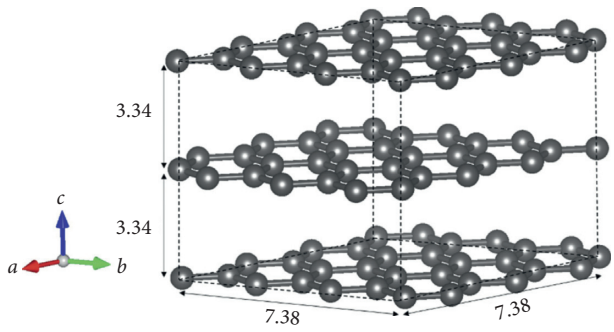

Figure 2: Geometry of perfect matrix graphite (0001) surface model obtained by full optimization.

out with a Gamma-centered $4 \times 4 \times 1$ k-mesh for (0001) surface. After optimization, the layer spacings of the perfect matrix graphite surface model are 3.34 Å that is close to the experimental value of 3.35 Å, as shown in Figure 2. Here, we also compared the graphite layer spacings obtained with and without vdW corrections and found that they are almost the same. This shows that although vdW correction can optimize the interlayer binding energy of graphite, it has little effect on the layer spacings. This may be due to the fact that the interlayer binding energy is too small to affect the layer spacing compared with the total energy of graphite system. Matrix graphite surfaces with single vacancy and interstitial are obtained by removing and adding one carbon atom from/to the perfect matrix graphite surface.

Cs, Sr, and Ag atoms were placed on top of each defective matrix graphite surfaces to find the most stable adsorption sites. The adsorption energies (E_{ads}) of adatoms were calculated following the equation $E_{ads} = E_{m/gra}/ - (E_m - E_{gra})$, where E_{gra} is the energy of defective or perfect supercells of matrix graphite surface, E_m is the energy of isolated Cs, Sr, and Ag atoms, and $E_{m/gra}$ is the total energy of matrix graphite surface supercell containing a metal fission atom. Note that $E_{ads} < 0$ corresponds to an atom more stable adsorbed on matrix graphite than as an isolated one.

3. Results and Discussion

3.1. Structures of Point Defects. Geometry structures of single vacancy and interstitial defects obtained by full optimization are shown in Figure 3. As we can see, interstitials in matrix graphite tend to form two different structures: "bridge" and "spiro" structures. The formation energies of "bridge" interstitial, "spiro" interstitial, and single vacancy defects are 6.77 eV, 5.52 eV, and 7.92 eV, respectively, which agree well with the experimental values [33–35] and other theoretical works [36–38]. The formation energies are calculated using the formula in [36]. Figure 3(a) shows the geometry of a "bridge" interstitial defect in matrix graphite. The distances from the adatom located below a C-C bond center to the carbon atoms connected to it are about 1.51 Å, implying that the adatom is chemically bound to the adjacent matrix graphite layer. Layer spacings of the matrix graphite with "bridge" interstitial defect are 4.31 Å and 3.42 Å, which are larger than the perfect matrix graphite. Figure 3(b) shows the geometry of a "spiro" interstitial defect in matrix graphite. The adatom and the atoms of two adjacent layers formed a tetrahedral geometry with a bond length of 1.49 Å. Compared with "bridge" defect structure, "spiro" defect structure has more sp3 bonds. Although there is the shear energy, formation energy of this "spiro" defect structure is lower than that of the "bridge" one by about 1.25 eV due to more covalent bonds formed between the interstitial and host atoms [36]. Layer spacings of the "spiro" interstitial defect are 3.43 Å and 3.40 Å, which are slightly larger than the perfect graphite. For graphite surface with "bridge" and "spiro" defects, interstitial carbon atoms destroy the planar structure of the graphite layer, which causes the graphite layer to produce pits at the interstitial atoms. Figure 3(c) shows the geometry of single vacancy defect in matrix graphite. Compared with "bridge" or "spiro" defect, single vacancy defect has less effect on the planar structure of the graphite layer, so that the graphite layer remains substantially flat. There is a dangling bond in the single vacancy defect. The presence of dangling bonds enhances chemical activity, which stabilizes other atoms in vacancy [39]. The matrix graphite surface with single vacancy defect is nearly geometrically flat. But the bond length of surface carbon atom is shorter than that of perfect matrix graphite one by about 0.03 Å. Layer spacings of the optimized system are 3.40 Å, which are consistent with the perfect matrix graphite.

3.2. Adsorption Energies of Cs, Sr, and Ag Atoms on Matrix Graphite Surface. Adsorption energies (E_{ads}) of metallic fission products of Cs, Sr, and Ag atoms on the preferred adsorption site of different matrix graphite surfaces are shown in Table 1. Figure 4 shows the corresponding atomic geometry structures of Cs, Sr, and Ag adsorbing on different types of matrix graphite surfaces. Luo et al. [16], Xia et al. [21], and Amft et al. [40] et al. believe that Cs, Sr, and Ag atoms prefer the hollow region (H site) at the center of the carbon hexagon for perfect graphite surface, while they prefer the defect region for defective graphite surface. Kuzenkova et al. showed that the interaction between graphene oxide (GO) and radionuclides takes place on the small holes or vacancy defects in the GO sheets [41]. In order to contrast with the adsorption energies of metallic fission products on defective graphite, it is first necessary to calculate the energies of fission products on perfect graphite. As shown in Table 1, matrix graphite surface with single vacancy has the strongest adsorption capacity for all three fission products, followed by matrix graphite surface with interstitial defect and perfect matrix graphite surface. Compared with perfect matrix graphite surface, the adsorption energy of Ag on matrix graphite surface with single vacancy defect is increased by nearly 8 times. It indicates that Ag atom is physically adsorbed on perfect matrix graphite surface, while it is chemically adsorbed on single vacancy defect structure. For "bridge" and "spiro" interstitial structures, different sp3/sp2 ratios show a slight difference in adsorption energies. The vertical distances (Z) between metal atoms and matrix graphite surfaces are shown in

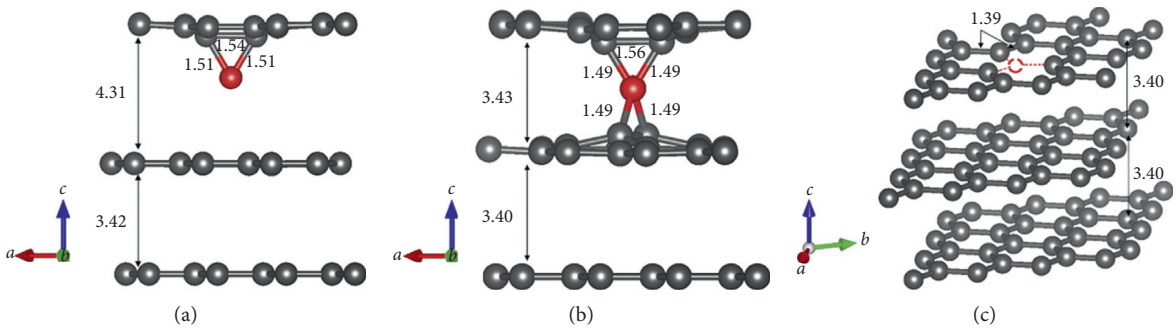

Figure 3: Geometries of vacancy and interstitial obtained by full optimization. (a) "Bridge" and (b) "spiro" interstitial structures in matrix graphite; (c) single vacancy on matrix graphite surface. Red balls represent the interstitial carbon atoms. All distances and bond lengths are in Å.

Table 1: Adsorption energies (E_{ads}) for perfect and defective matrix graphite (unit: eV).

Structures	Cs		Sr		Ag	
	E_{ads}	Z	E_{ads}	Z	E_{ads}	Z
Perfect matrix graphite	−1.88	2.59	−1.46	2.27	−0.27	2.87
"Bridge" interstitial defect	−2.50	2.32	−2.33	1.82	−0.39	2.22
"Spiro" interstitial defect	−2.25	2.21	−2.13	1.83	−0.40	2.48
Single vacancy defect	−2.83	2.52	−3.37	2.01	−2.37	1.68

Z: the vertical distance between metal atoms and matrix graphite surface; unit is Å.

Table 1. Since the defective graphite surfaces have stronger adsorption capacity for metal atoms, the corresponding Z-values are smaller, which is consistent with the results of adsorption energy. However, for Cs and Sr atoms, Z-value corresponding to the graphite surface with single vacancy defect is larger than graphite with "bridge" and "spiro" defects. This is because single vacancy defect's geometry change is slight, but "bridge" and "spiro" defects form a pit hole. For Ag atom, adsorption capacity of single vacancy defect is much larger than "bridge" or "spiro" defect, so the corresponding Z-value is smaller. All these results suggest that the presence of dangling bond as well as sp3 bond favors stronger binding than a pure sp2 structure.

Results in Table 1 also show that both Cs and Sr have stronger adsorption capacities than Ag, whether it is on a perfect matrix graphite surface or a defective matrix graphite surface. It is noted that Cs adsorbs stronger than Sr on perfect matrix graphite surface and matrix graphite surface with interstitial defect. On the contrary, Sr adsorbs stronger than Cs on matrix graphite surface with single vacancy defect. It can be inferred that the retention of Sr and Cs by matrix graphite is determined by its surface morphology, e.g., sp3/sp2 ratios and dangling bond. The surface morphology of matrix graphite has a more obvious effect on the adsorption of Ag. This result may guide us to improve the manufacturing method of matrix graphite and to produce matrix graphite with more defects so as to retain more metallic fission products.

3.3. Electronic Structure Analysis. For further analysis of adsorption behaviors between fission products and matrix graphite structure, the electronic structure of the adsorption system is calculated. The charge density difference (CDD) values are calculated as $\Delta\rho_{m/gra} = \rho_{m/gra}/ - (\rho_m - \rho_{gra})$ by using the VESTA software [42], where $\rho_{m/gra}$ is the charge density of adsorption system, ρ_m is the charge density of a metal atom, and ρ_{gra} is the charge density of a matrix graphite supercell. Note that in calculation of the latter two quantities, the atomic positions are fixed as those in the adsorption system. Figure 5 shows CDD of Ag, Cs, and Sr atoms adsorption on perfect matrix graphite surface. When the value of CDD is positive, it means that the charge density in the adsorption system is greater than the charge density value obtained by the original electron overlap, that is, the gain of electrons; when the value of CDD is negative, it means the charge density in the adsorption system is smaller than the charge density value obtained by the original electron overlap, that is, the loss of electrons. Figure 5(a) shows that there is nearly no electron transfer between Ag and perfect matrix graphite surface. It indicates that Ag is physically adsorbed on perfect matrix graphite surface, which is consistent with the adsorption energy results. Figures 5(b) and 5(c) show that Cs and Sr atoms transfer electrons to perfect matrix graphite surface because of weaker electronegativity than C atom [14]. It indicates that the perfect matrix graphite surface has stronger adsorption capacity for Cs and Sr than Ag.

Charge density difference (CDD) of fission products of Ag, Cs, and Sr adsorbed on defective matrix graphite surface is analyzed, as shown in Figures 6 and 7. It can be seen that there is more electrons' transfer between fission products and single vacancy defect (see Figure 7) than between "bridge" and "spiro" interstitial defects (see Figure 6), which is consistent with the tendency of adsorption energy (see Table 1). Figure 6(a) shows that there are few electrons

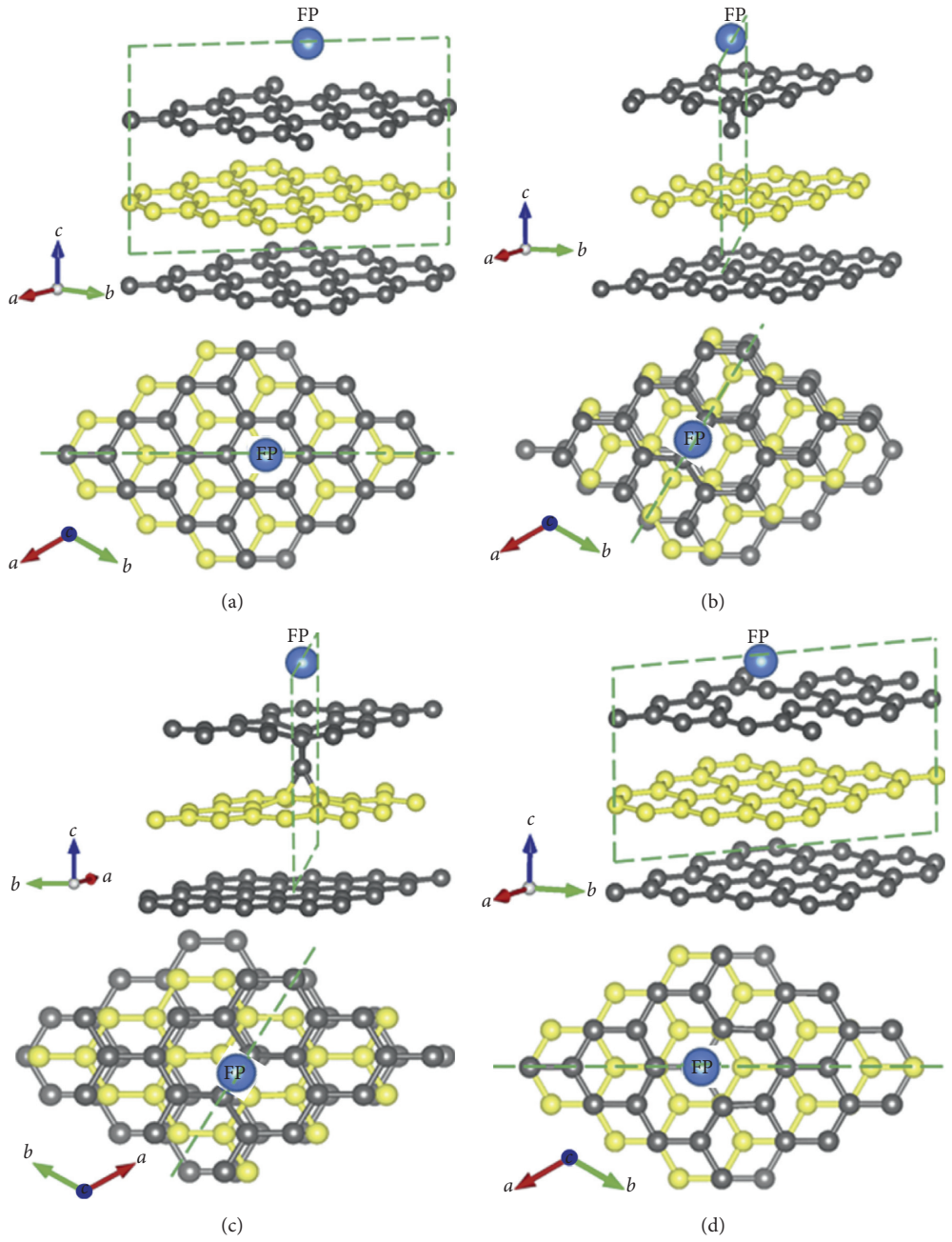

FIGURE 4: Geometry structures of metal fission product adsorbed on matrix graphite surface: (a) perfect matrix graphite surface; (b) "bridge" and (c) "spiro" interstitial defects; and (d) single vacancy defect. Yellow balls represent the second layer of carbon atoms. Blue balls represent the metal fission products. The dash green lines represent the cross-sectional lines of charge density difference.

transfer between Ag and "bridge" interstitial defect. Figure 6(d) shows that Ag partial orbitals gain electrons from "spiro" interstitial defect. Figures 6(b)-6(c) show that both the interstitial and carbon atoms adjacent to fission products gain electrons from Cs or Sr. Figures 6(e)-6(f) show that the interstitials suffer a loss of electron while carbon atoms gain of electrons from Cs or Sr atoms. Figure 7 also shows that electrons' transfer between fission products and single vacancy defect are limited to a narrow region. And electrons mainly transfer to three nearest neighbor carbon atoms from fission products.

To learn more about adsorption behaviors, we calculate the density of state (DOS) of different adsorption system using a $16 \times 16 \times 1$ k-mesh, and the energy eigenvalues are smeared with Gaussians of width $\sigma = 0.05$ eV. In the plots, the energy levels are aligned through Dirac points. Figure 8 shows the DOS of matrix graphite with different defects. It can be seen from Figures 8(a) and 8(b) that the DOS of graphite with "bridge" defect is almost the same as that of

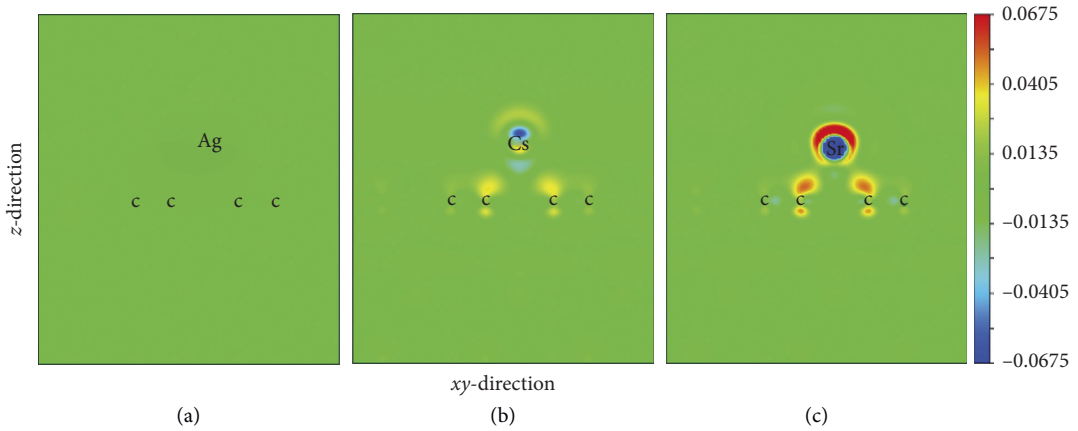

FIGURE 5: Charge density difference (CDD) based on the green bash lines shown in Figure 4(a) of fission products on perfect matrix graphite surface. (a) Ag; (b) Cs; and (c) Sr. Red and blue areas represent positive and negative charge differences. Isosurface level was set at 0.0069e/Å^3.

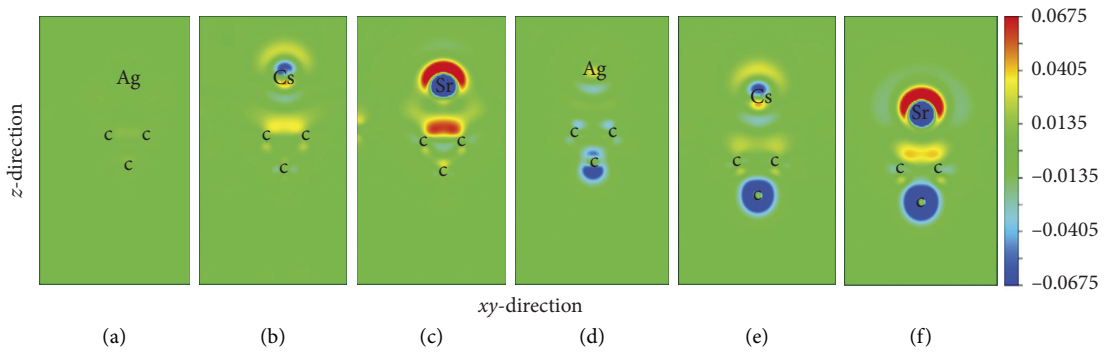

FIGURE 6: Charge density difference (CDD) based on the green bash lines shown in Figures 4(b) and 4(c) of Ag, Cs, and Sr on matrix graphite surface. (a–c) Matrix graphite surface with "bridge" defect; (d–f) matrix graphite surface with "spiro" defect. Red and blue areas represent positive and negative charge differences. Isosurface level was set at 0.0069e/Å^3.

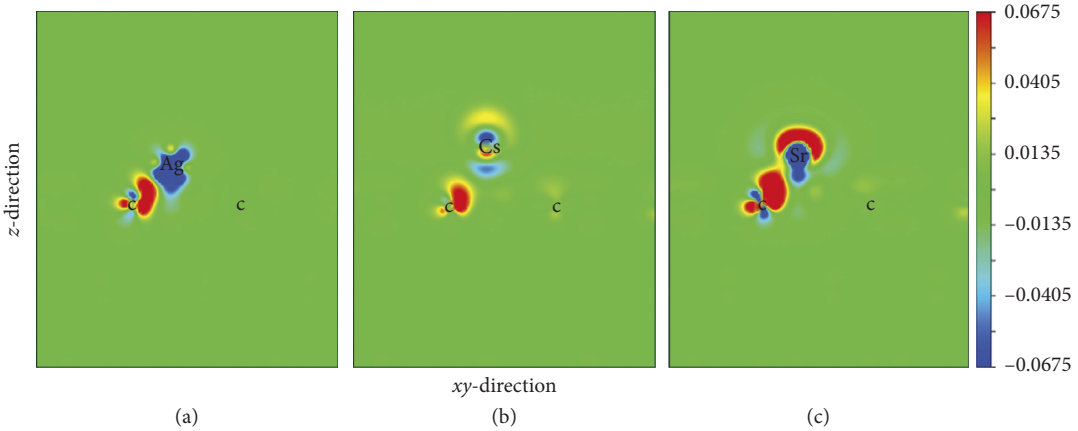

FIGURE 7: Charge density difference (CDD) based on the green bash lines shown in Figure 4(d) of Ag, Cs, and Sr on matrix graphite surface with single vacancy defect. (a) Ag; (b) Cs; and (c) Sr. Red and blue areas represent positive and negative charge differences. Isosurface level was set at 0.0069e/Å^3.

perfect graphite, and the peak value is sharper than that of graphite with "spiro" or vacancy defects. For graphite with "spiro" and vacancy defects, sharp peaks appear in the DOS near the Fermi level, corresponding to the defect states of graphite. In contrast, the "bridge" defect has the least effect on the electronic structure of matrix graphite, while single

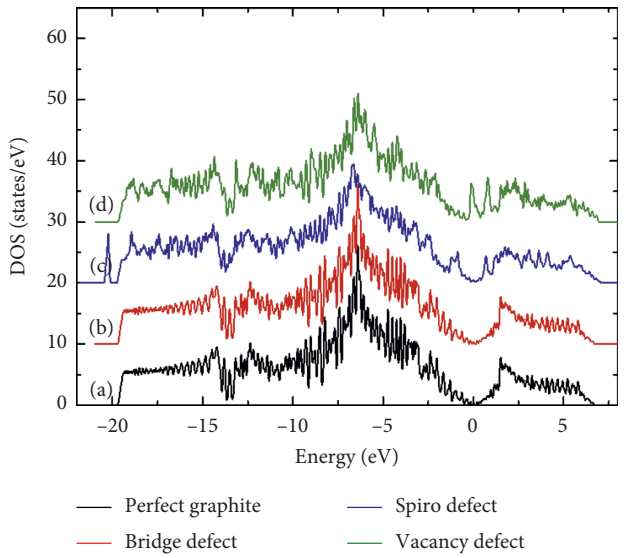

Figure 8: The DOS of matrix graphite with different defects: (a) perfect graphite; (b) "bridge" defect; (c) "spiro" defect; (d) single vacancy defect. The energy is relative to Fermi level (E_f) at $E = 0$ eV.

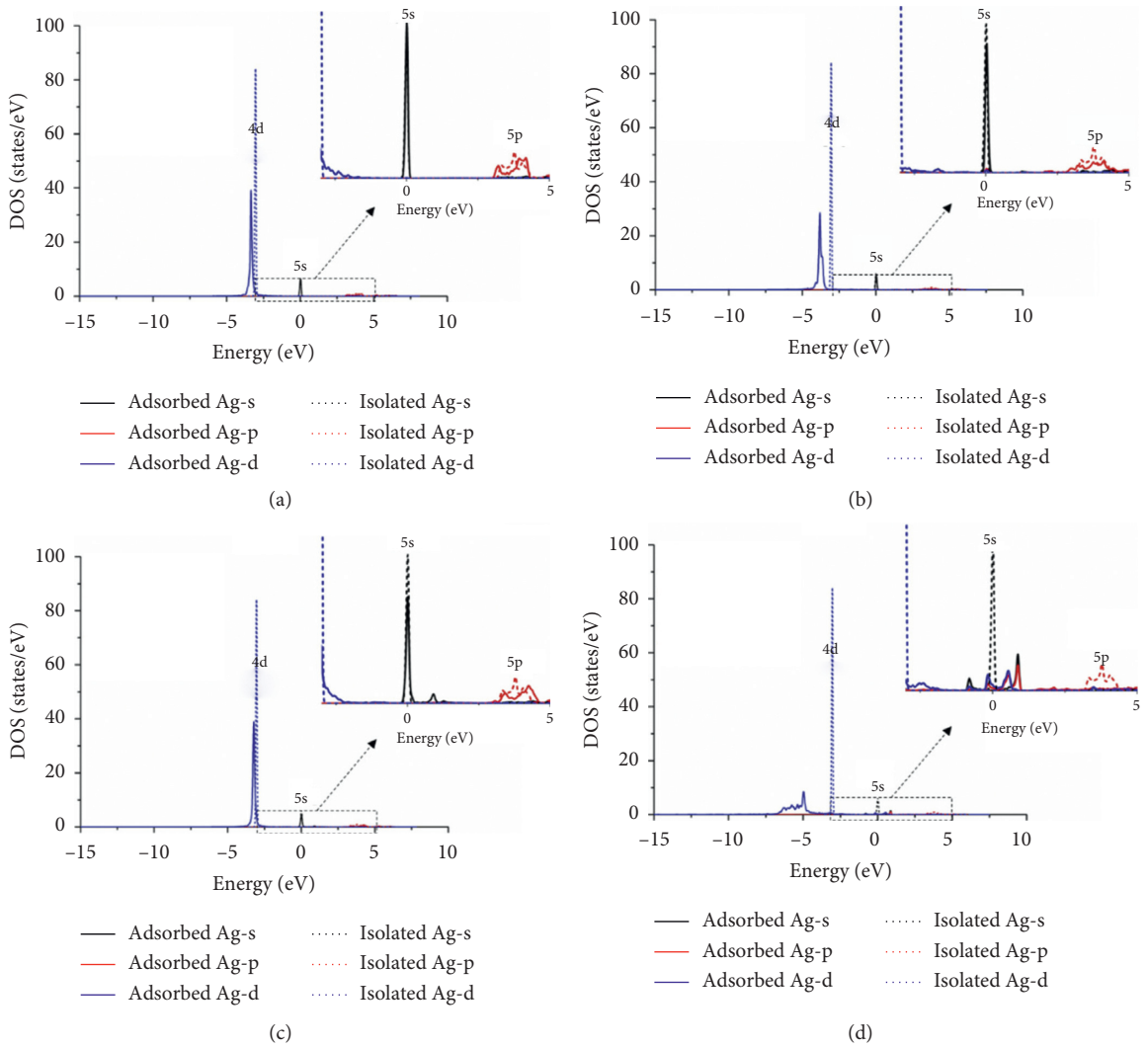

Figure 9: The DOS for isolated Ag atom (dashed line) and Ag adsorbed on matrix graphite surface (solid line): (a) perfect matrix graphite surface; (b) "bridge" interstitial defect; (c) "spiro" interstitial defect; (d) single vacancy defect. The energy is relative to Fermi level (E_f) at $E = 0$ eV.

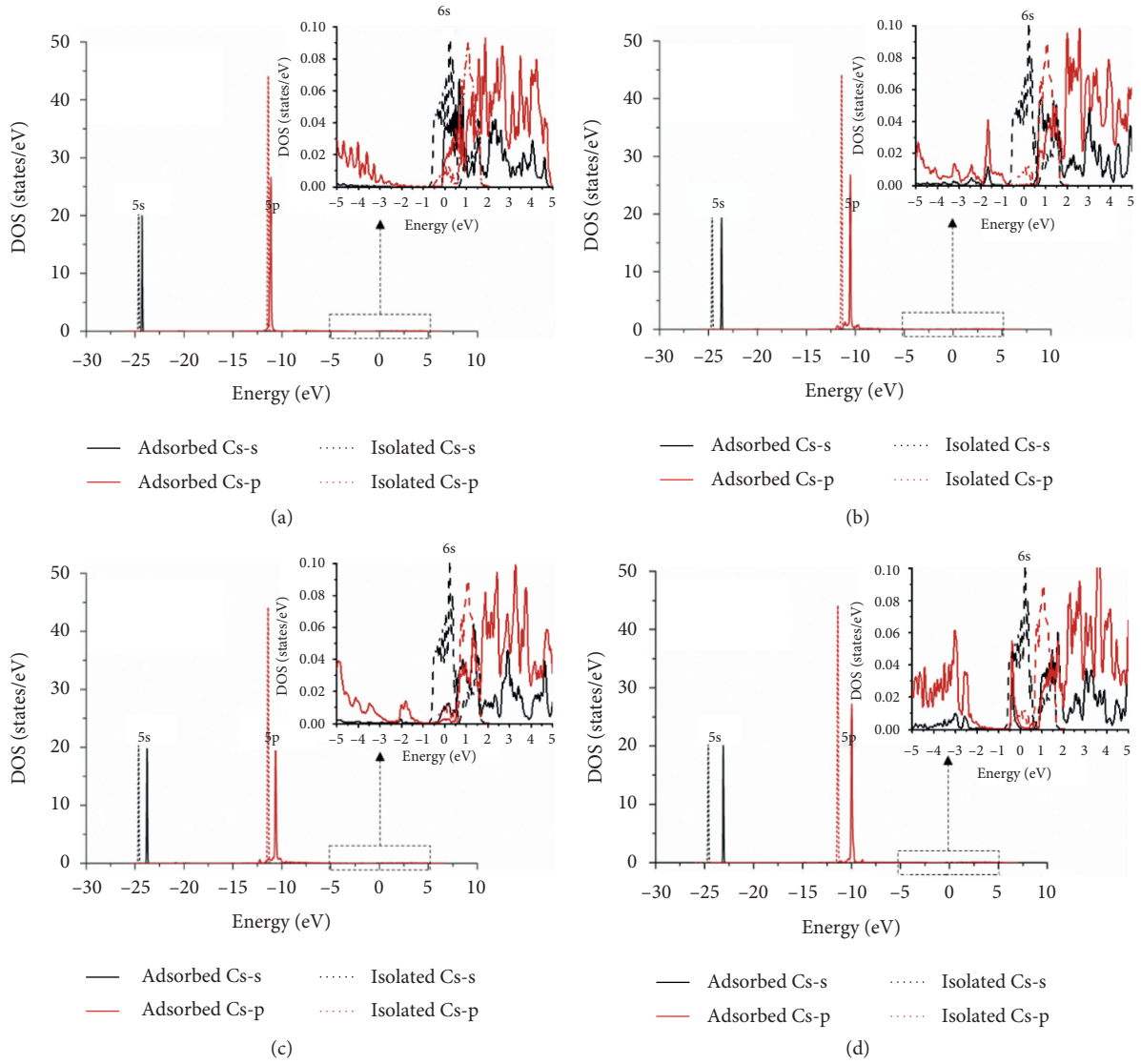

FIGURE 10: The DOS for isolated Cs atom (dashed line) and Cs adsorbed on matrix graphite surface (solid line): (a) perfect matrix graphite surface; (b) "bridge" interstitial defect; (c) "spiro" interstitial defect; (d) single vacancy defect. The energy is relative to Fermi level (E_f) at $E = 0$ eV.

vacancy defect significantly alters the matrix graphite electronic structure.

Figure 9 shows the 4d, 5s, and 5p orbits of isolated Ag atom (dashed line) and adsorbed Ag atoms (solid line). It is seen from Figure 9(a) that the shape and peak position of DOS of isolated and adsorbed Ag atom are almost the same, which indicates no electron transfers between Ag and the perfect matrix graphite surface. When interstitial defects are introduced, Ag atoms have stronger interaction with defective matrix graphite surface. However, there are different interactions between Ag atoms and matrix graphite surface for different interstitial defects, while their adsorption capacity is similar. It can be seen from Figure 9(b) that the 4d states of Ag atom shift slightly toward a lower energy direction when Ag adsorbed on matrix graphite with "bridge" defect. Moreover, the DOS of 5s for Ag atom are delocalized and partial density moves above the Fermi level at ~1 eV when Ag adsorbed on matrix graphite with "spiro" defect. It can be seen from Figure 9(d) that the DOS of 4d and 5p has a noticeable broadening and the majority of density shifts toward a lower energy direction when Ag atom adsorbed on matrix graphite with vacancy defect. The DOS of full 5s for adsorbed Ag are delocalized as compared with isolated Ag atom. Remarkably, although the majority of 5s states move above Fermi level, there are still some 5s states below Fermi level, which indicates that Ag atom not only loses electrons to graphite but also gains some electrons from graphite. This is because the electrochemistry of Ag atom is close to C atom, and there exists resonance between 5s state and graphite when partial electrons lose to graphite with vacancy [19]. Moreover, there is strong hybridization of 4d, 5s, and 5p states of adsorbed Ag, which is easier to form covalent bonding with matrix graphite [43].

Figure 10 shows the DOS of isolated Cs atom and Cs adsorbed on matrix graphite surface with different defects. The 5s, 5p, and 6s states of Cs atom have a noticeable upshift

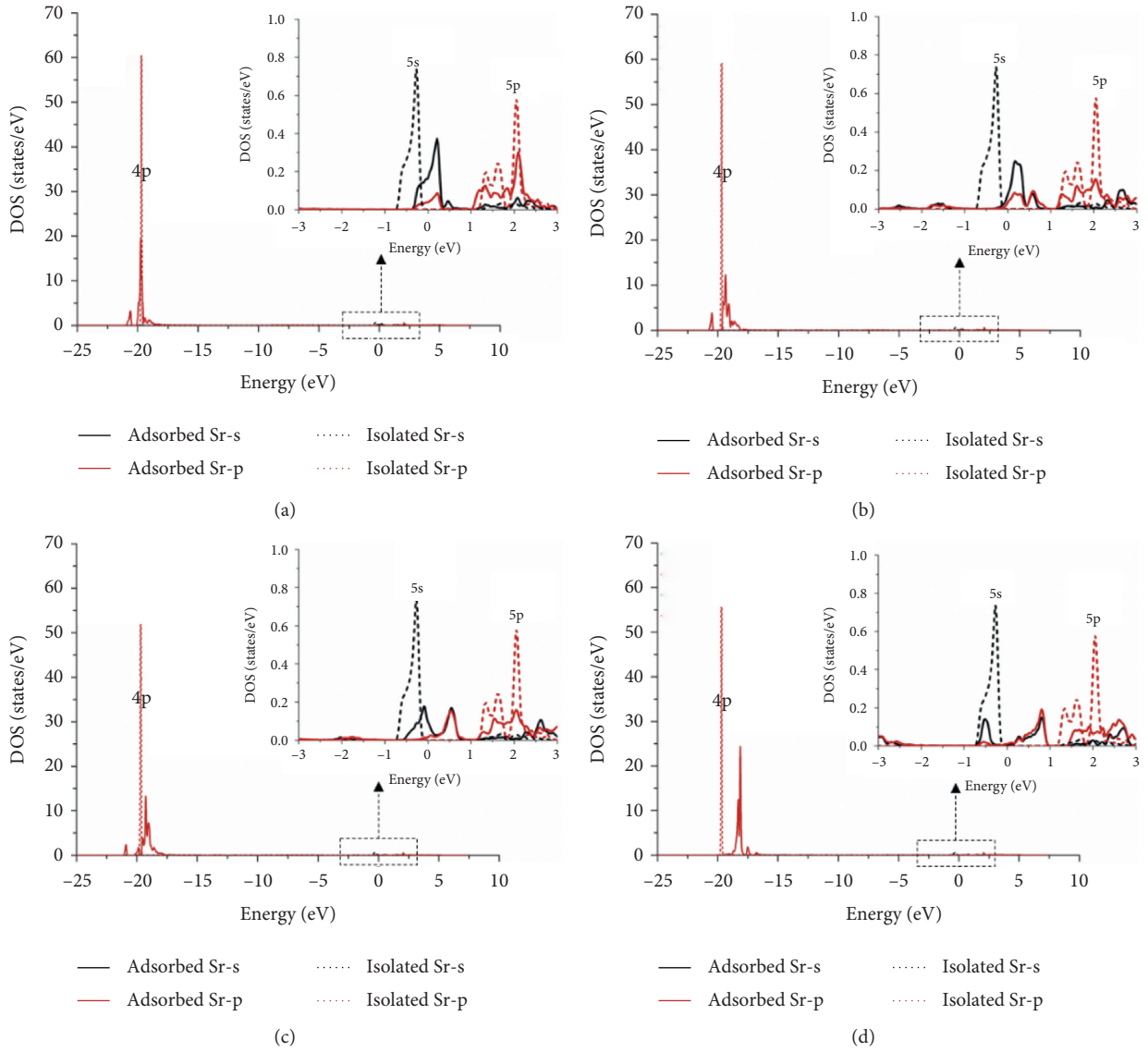

Figure 11: The DOS for isolated Sr atom (dashed line) and Sr adsorbed on matrix graphite surface (solid line): (a) perfect matrix graphite surface; (b) "bridge" interstitial defect; (c) "spiro" interstitial defect; (d) single vacancy defect. The energy is relative to Fermi level (E_f) at $E = 0$ eV.

relative to the Fermi level, but the degrees of upshift are different for different types of matrix graphite surface. It is noted that part of 6s and 5p states moves above the Fermi level, which indicates that the electrons of Cs transferred to matrix graphite surface. For Cs adsorbed on perfect matrix graphite surface (see Figure 10(a)), partial 6s states move above the Fermi level. For Cs adsorbed on defective matrix graphite surface (see Figures 10(b)–10(d)), full 6s states move above the Fermi level. It indicates that matrix graphite with defects tends to form stronger bonds with Cs atom than the perfect matrix graphite. This result is well consistent with the results of adsorption energies.

For the Sr adsorbed systems, as shown in Figure 11, the result of DOS is similar to Cs. The 4p and 5s states have a noticeable broadening and upshift relative to the Fermi level as shown in Figure 11(a), which indicates that Sr transfer electrons to matrix graphite. For Sr adsorbed on matrix graphite surface with bridge and spiro defects (see Figures 11(b) and 11(c)), there are different behaviors between the 5s states of Ag atom and matrix graphite. The 5s states are delocalized and there is hybridization between 5s and 5p states, which exhibit more covalent bonding characteristics for Ag adsorbed on matrix graphite with spiro defect. Moreover, there are stronger hybridization of 5s and 5p states of adsorbed Sr on matrix graphite with single vacancy defect, suggesting that there is a stronger interaction between Sr and matrix graphite with single vacancy defect.

4. Conclusions

In this work, DFT methods were employed to examine several interstitial defects for matrix graphite. Adsorption energies

and electronic structures for Cs, Sr, and Ag on matrix graphite surfaces with defects were calculated and analyzed. Fission products adsorbed stronger on defective matrix graphite surfaces than the perfect matrix graphite surfaces, indicating dangling bonds and sp3 bonds play a critical role in the adsorption behavior of Cs, Sr, and Ag on matrix graphite. Matrix graphite surface with single vacancy defects has a stronger adsorption capacity for fission products than that with interstitial defects. Although the matrix graphite with "bridge" and "spiro" defects has similar adsorption capacity for metallic fission products, their interaction behaviors are completely different due to different electronic structure. It is also observed that Cs and Sr adsorb stronger than Ag on matrix graphite surfaces, which indicates that the retention of Sr and Cs by matrix graphite is stronger than that of Ag. This result is consistent with the electronegativity of metal atoms relative to the carbon atom. Transition metal atoms, such as Ag atom, exhibit covalent bonding characteristics because their electronegativity is close to that of carbon atom. These results are helpful for predicting and understanding the diffusion capacity and path of metallic fission products on the matrix graphite of HTGR.

Data Availability

No data were used to support this study.

Conflicts of Interest

The authors declare that they have no conflicts of interest regarding the publication of this paper.

Acknowledgments

This work was supported by the National S&T Major Project (Grant no. ZX06901).

References

[1] C. H. Tang, Y. P. Tang, J. G. Zhu, Y. W. Zou, J. H. Li, and X. J. Ni, "Design and manufacture of the fuel element for the 10 MW high temperature gas-cooled reactor," *Nuclear Engineering and Design*, vol. 218, no. 1–3, pp. 91–102, 2002.

[2] K. Sawa and S. Ueta, "Research and development on HTGR fuel in the HTTR project," *Nuclear Engineering and Design*, vol. 233, no. 1–3, pp. 163–172, 2004.

[3] S. Yeo and Y.-W. Lee, "Reduced anisotropic properties of Cold Isostatic Pressed graphite matrix compacts," *Journal of Nuclear Materials*, vol. 515, pp. 245–256, 2019.

[4] Y. Z. Liu and J. Z. Cao, "Fission product release and its environment impact for normal reactor operations and for relevant accidents," *Nuclear Engineering and Design*, vol. 218, no. 1–3, pp. 81–90, 2002.

[5] J. W. Prados and J. L. Scott, "Mathematical model for predicting coated-particle behavior," *Nuclear Applications*, vol. 2, no. 5, pp. 402–414, 1966.

[6] G. K. Miller, D. A. Petti, D. J. Varacalle, and J. T. Maki, "Consideration of the effects on fuel particle behavior from shrinkage cracks in the inner pyrocarbon layer," *Journal of Nuclear Materials*, vol. 295, no. 2-3, pp. 205–212, 2001.

[7] J. T. Maki, D. A. Petti, D. L. Knudson, and G. K. Miller, "The challenges associated with high burnup, high temperature and accelerated irradiation for TRISO-coated particle fuel," *Journal of Nuclear Materials*, vol. 371, no. 1-3, pp. 270–280, 2007.

[8] J. Drowart, G. De Maria, and M. G. Inghram, "Thermodynamic study of sic utilizing a mass spectrometer," *The Journal of Chemical Physics*, vol. 29, no. 5, pp. 1015–1021, 1958.

[9] W. Schenk and H. Nabielek, "High-temperature reactor fuel fission product release and distribution at 1600 to 1800°C," *Nuclear Technology*, vol. 96, no. 3, pp. 323–336, 1991.

[10] A. Londono-Hurtado, I. Szlufarska, R. Bratton, and D. Morgan, "A review of fission product sorption in carbon structures," *Journal of Nuclear Materials*, vol. 426, no. 1–3, pp. 254–267, 2012.

[11] H. S. Zhao, T. X. Liang, J. Zhang, J. He, Y. W. Zou, and C. H. Tang, "Manufacture and characteristics of spherical fuel elements for the HTR-10," *Nuclear Engineering and Design*, vol. 236, no. 5-6, pp. 643–647, 2006.

[12] J. Ma, D. Alfe, A. Michaelides, and E. Wang, "Stone-Wales defects in graphene and other planarsp2-bonded materials," *Physical Review B*, vol. 80, no. 3, 2009.

[13] B. L. Holian, "The interaction between cesium and graphite for use in the study of surface phenomena," in *Proceedings of the 1976 International Conference on Computer Simulation for Materials Applications*, pp. 233–244, Gaithersburg, Maryland, April 1976.

[14] K. Nakada and A. Ishii, *DFT Calculation for Adatom Adsorption on Graphene, Graphene Simulation*, pp. 3–20, Intech Europe, Rijeka, Croatia, 2011.

[15] W. Kohn and L. J. Sham, "Self-consistent equations including exchange and correlation effects," *Physical Review*, vol. 140, no. 4A, p. 1133, 1965.

[16] X. Luo, C. Fang, X. Li, W. Lai, L. Sun, and T. Liang, "Study of interaction between radioactive nuclides and graphite surface by the first-principles and statistic physics," *Applied Surface Science*, vol. 285, pp. 278–286, 2013.

[17] C. Li and C. Fang, "First-principle studies of radioactive fission productions of Cs/Sr/Ag/I adsorption on silicon carbide in HTGR," *Progress in Nuclear Energy*, vol. 100, pp. 164–170, 2017.

[18] H. Y. Chen, H. Li, C. Li, J. Z. Cao, and C. Fang, "Diffusion behaviors of hydrogen isotopes in incoloy 800H: a first-principles study," *Science and Technology of Nuclear Installations*, vol. 2017, Article ID 4038021, 6 pages, 2017.

[19] W. Y. Wang, C. Li, J. Z. Cao, and C. Fang, "Adsorption behaviors of cobalt on the graphite and SiC surface: a first-principles study," *Science and Technology of Nuclear Installations*, vol. 2017, pp. 1–8, 2017.

[20] A. Londono-Hurtado, D. Morgan, and I. Szlufarska, "First-principles study of Cs and Sr sorption on carbon structures," *Journal of Applied Physics*, vol. 111, no. 9, Article ID 094912, 2012.

[21] D. Xia, C. Ren, W. Zhang et al., "Theoretical study of the interaction between metallic fission products and defective graphite," *Computational Materials Science*, vol. 106, pp. 129–134, 2015.

[22] G. Kresse and J. Hafner, "Ab initiomolecular dynamics for open-shell transition metals," *Physical Review B*, vol. 48, no. 17, pp. 13115–13118, 1993.

[23] J. P. Perdew, K. Burke, and M. Ernzerhof, "Generalized gradient approximation made simple," *Physical Review Letters*, vol. 77, no. 18, pp. 3865–3868, 1996.

[24] S. Lebegue, J. Harl, T. Gould, J. G. Angyan, G. Kresse, and J. F. Dobson, "Cohesive properties and asymptotics of the dispersion interaction in graphite by the random phase Approximation," *Physical Review Letters*, vol. 105, no. 19, 2010.

[25] M. Dion, H. Rydberg, E. Schroder, D. C. Langreth, and B. I. Lundqvist, "Van der Waals density functional for general geometries," *Physical Review Letters*, vol. 92, no. 24, p. 4, 2004.

[26] S. Grimme, "Semiempirical GGA-type density functional constructed with a long-range dispersion correction," *Journal of Computational Chemistry*, vol. 27, no. 15, pp. 1787–1799, 2006.

[27] S. Grimme, J. Antony, S. Ehrlich, and H. Krieg, "A consistent and accurate ab initio parametrization of density functional dispersion correction (DFT-D) for the 94 elements H-Pu," *The Journal of Chemical Physics*, vol. 132, no. 15, Article ID 154104, 19 pages, 2010.

[28] S. Grimme, S. Ehrlich, and L. Goerigk, "Effect of the damping function in dispersion corrected density functional theory," *Journal of Computational Chemistry*, vol. 32, no. 7, pp. 1456–1465, 2011.

[29] A. Tkatchenko and M. Scheffler, "Accurate molecular van der Waals interactions from ground-state electron density and free-atom reference data," *Physical Review Letters*, vol. 102, no. 7, p. 4, 2009.

[30] A. Tkatchenko, R. A. DiStasio, R. Car, and M. Scheffler, "Accurate and efficient method for many-body van der Waals interactions," *Physical Review Letters*, vol. 108, no. 23, p. 5, 2012.

[31] T. Bucko, S. Lebegue, T. Gould, and J. G. Angyan, "Many-body dispersion corrections for periodic systems: an efficient reciprocal space implementation," *Journal of Physics: Condensed Matter*, vol. 28, no. 4, Article ID 045201, 2016.

[32] L. A. Girifalco and R. A. Lad, "Energy of cohesion, compressibility, and the potential energy functions of the graphite system," *The Journal of Chemical Physics*, vol. 25, no. 4, pp. 693–697, 1956.

[33] A. Hashimoto, K. Suenaga, A. Gloter, K. Urita, and S. Iijima, "Direct evidence for atomic defects in graphene layers," *Nature*, vol. 430, no. 7002, pp. 870–873, 2004.

[34] F. Banhart, "Irradiation effects in carbon nanostructures," *Reports on Progress in Physics*, vol. 62, no. 8, pp. 1181–1221, 1999.

[35] P. A. Thrower and R. M. Mayer, "Point defects and self-diffusion in graphite," *Physica Status Solidi (a)*, vol. 47, no. 1, pp. 11–37, 1978.

[36] H. Zhang, M. Zhao, X. Yang, H. Xia, X. Liu, and Y. Xia, "Diffusion and coalescence of vacancies and interstitials in graphite: a first-principles study," *Diamond and Related Materials*, vol. 19, no. 10, pp. 1240–1244, 2010.

[37] L. Li, S. Reich, and J. Robertson, "Defect energies of graphite: density-functional calculations," *Physical Review B*, vol. 72, no. 18, 2005.

[38] C. D. Latham, M. I. Heggie, J. A. Gamez, I. Suarez-Martinez, C. P. Ewels, and P. R. Briddon, "The di-interstitial in graphite," *Journal of Physics: Condensed Matter*, vol. 20, no. 39, Article ID 395220, 2008.

[39] W. Zhang, L. T. Sun, Z. J. Xu et al., "Migration of gold atoms in graphene ribbons: role of the edges," *Physical Review B*, vol. 81, no. 12, 2010.

[40] M. Amft, S. Lebegue, O. Eriksson, and N. V. Skorodumova, "Adsorption of Cu, Ag, and Au atoms on graphene including van der waals interactions," *Journal of Physics; Condensed Matter*, vol. 23, no. 39, Article ID 395001, 2011.

[41] A. S. Kuzenkova, A. Y. Romanchuk, A. L. Trigub et al., "New insights into the mechanism of graphene oxide and radionuclide interaction," *Carbon*, vol. 158, pp. 291–302, 2019.

[42] K. Momma and F. Izumi, "VESTA 3 for three-dimensional visualization of crystal, volumetric and morphology data," *Journal of Applied Crystallography*, vol. 44, no. 6, pp. 1272–1276, 2011.

[43] K. T. Chan, J. B. Neaton, and M. L. Cohen, "First-principles study of metal adatom adsorption on graphene," *Physical Review B*, vol. 77, no. 23, p. 12, 2008.